Structure and properties of mesoporous alumino-phosphoro-vanadates

Konstadina M. Kolonia,[a] Dimitris E. Petrakis,[a] Thomas N. Angelidis,[b] Pantelis N. Trikalitis[a] and Philippos J. Pomonis*[a]

[a]*Department of Chemistry, University of Ioannina 45332, Greece*
[b]*Department of Chemistry, University of Thessaloniki, Thessaloniki 54006, Greece*

Mesoporous solids of the general formula $Al_{100}P_xV_y$-600, where $x, y = 0, 5, 10, 20$; and 600 corresponds to the final firing temperature (°C), have been prepared and characterized by X-ray diffraction (XRD), surface area and porosity measurements and SEM/EDX analysis. The incorporation of P and/or V into the original $Al_{100}P_0V_0$ solid results in increase of the specific surface area (ssa) from 200 to 390 $m^2\ g^{-1}$ and the pore volume from 0.43 to 1.19 $cm^3\ g^{-1}$. The maximum effect is resulted by P rather than V while a synergistic action of the two is apparent which is maximized at *ca.* 15% cumulative addition of the two elements. The highest ssa appears in the $Al_{100}P_{10}V_5$ solid while the narrowest pore size distribution (p.s.d.), as described by its full width at half maximum (FWHM), appears in $Al_{100}P_0V_5$ solid for which FWHM = 2.1 nm. The p.s.d. of the solids is approximated by a mixed Gaussian and Lorentzian component which varies in a controllable manner by the P and/or V addition. The XRD results show that $Al_{100}P_0V_0$ possesses the γ-Al_2O_3 structure but the samples become gradually amorphous upon addition of P and/or V up to $Al_{100}P_{10}V_{10}$, while in the samples containing 20% P and/or V the crystal phases of $AlPO_4$ and V_2O_5 become apparent. SEM shows that the surface of the crystallites becomes more fragmented by the addition of P and/or V up to 10% addition while 20% addition results in a layered appearance of the crystallite external surface. EDX analysis shows that phosphorus is accumulated on the surface to an amount of around 30–40% for low concentration of P and/or V and 10–20% for higher concentrations. For vanadium the emerging picture is less clear, although some accumulation is detected, a fact due to non-homogeneous distribution of V on the external surface of the mesoporous solids.

The synthesis of the highly ordered mesoporous silicate/aluminosilicate materials M41S/MCM-41 in 1992 by the Mobil group,[1,2] offered to the scientific community a novel approach in the synthesis of such solids and created a interdisciplinary field of research in the domain of self-organized matter. Such structures extend the range of microporous molecular-sieve materials into the mesoporous region but perhaps more important is the fact that, if the original synthetic approach can be extended to other transition-metal oxide mesostructures, the resulting nanocomposites might find applications as solid-electrolyte devices,[3,4] as substrates for biochemical separations[5] and as high surface area redox catalysts[6] for reactions like methane oxidation, NO_x decomposition, hydrodesulfurization, photocatalytic decomposition of organic halides and solid-acid catalysis.[7] Another reason which makes this new chemistry particularly promising is that it leads to novel chemical routes for the fabrication of biomimetic inorganic materials with organized hierarchical structure and form, analogous to the biomineralized architectures fashioned by many single-celled organisms.[8,9] Relevant advances in the recent literature include the preparation of mesoporous zirconium oxide,[10,11] of porous zirconium oxo-phosphates,[12] of mesoporous titanium-substituted silicates[13] as well as mesoporous titanium oxide,[14] and finally of mesoporous niobium oxide.[7] Workers interested in these subjects can find a critical discussion in the articles by Behrens[15] and Behrens and Stucky[16] while important relevant information exists in ref. 17 on the generalized synthesis of periodic surfactant–inorganic composite materials, in ref. 18 on the templating routes to mesoporous molecular sieves as well as in ref. 19 on the mechanism of formation of inorganic–organic interfaces during the synthesis of silicate mesostructures. The level of knowledge on mesoporous solids previous to the invention of M41S/MCM-41 materials[1,2] is summarized in a volume edited in 1993.[20]

Table 1 Surface areas, pore volumes and pore sizes of the $Al_{100}P_xV_y$ solids. The % Gauss (G) and Lorentz (L) contribution to the pore size distribution, the centre and the FWHM of the p.s.d. and the χ^2 criterion of fitting is also listed

sample	surface area (BET)/$m^2\ g^{-1}$	pore volume (BJH)/$cm^3\ g^{-1}$	mean pore diameter/nm	%G	%L	centre of p.s.d./nm	FWHM/nm	χ^2
$Al_{100}P_0V_0$	201.3	0.430	8.5	70	30	6.54	2.5	0.00647
$Al_{100}P_0V_5$	270.5	0.446	6.6	60	40	5.44	2.1	0.00532
$Al_{100}P_0V_{10}$	301.9	0.497	6.6	70	30	5.24	2.1	0.01109
$Al_{100}P_0V_{20}$	176.7	0.456	10.3	0	100	8.14	5.2	0.00074
$Al_{100}P_5V_0$	245.3	0.518	8.4	55	45	6.34	2.4	0.00523
$Al_{100}P_5V_5$	352.6	0.703	8.0	55	45	6.24	2.9	0.01817
$Al_{100}P_5V_{10}$	359.0	0.833	9.3	30	70	6.94	3.4	0.02306
$Al_{100}P_5V_{20}$	286.3	0.743	10.4	20	80	7.34	4.1	0.02038
$Al_{100}P_{10}V_0$	319.8	1.192	14.0	35	65	9.14	4.4	0.03759
$Al_{100}P_{10}V_5$	386.1	1.146	11.9	20	80	9.24	4.6	0.03123
$Al_{100}P_{10}V_{10}$	321.5	1.109	13.8	20	80	10.24	5.4	0.02712
$Al_{100}P_{10}V_{20}$	305.2	1.020	13.4	0	100	9.24	6.0	0.01949
$Al_{100}P_{20}V_0$	239.5	0.928	15.5	15	85	10.74	6.3	0.01850
$Al_{100}P_{20}V_5$	336.0	0.475	5.7	10	90	10.34	5.9	0.02527
$Al_{100}P_{20}V_{10}$	257.9	0.358	5.6	0	100	12.44	10.2	0.00251
$Al_{100}P_{20}V_{20}$	199.9	0.245	4.9	0	100	12.64	10.3	0.00191

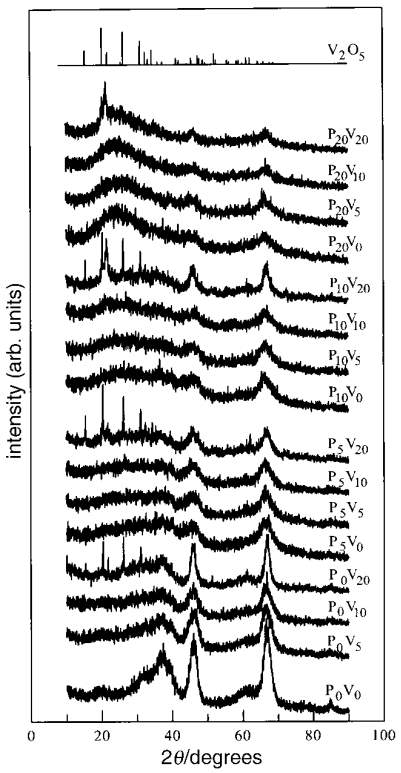

Fig. 1 XRD patterns of the Al—P—V—O mesoporous solids heated at 600 °C

The present work is referred to some recent results on mesoporous alumino-phosphoro-vanadate solids and is a follow-up of two other recent publications on aluminophosphate solids.[21,22] Such solids are prepared *via* decomposition of an ammonium nitrate precursor, rather than an organic template and the pore size distribution of the resulting solids, which is centered in the mesoporous region, varies in a controllable manner depending on the amount of phosphorus in the solids. Also, such aluminophosphates possess a Bronsted and/or Lewis acidity which is directly related to the phosphate groups on their surface. The reason which led us to the extension of aluminophosphates to alumino-phosphoro-vanadates is that vanadium, like phosphorus, exists in a pentavalent oxidation state and since phosphorus is accumulated on the surface of alumina leading to an increased surface area and narrow pore size distribution, we decided to study the corresponding behaviour of vanadium.

Experimental and Results

Preparation of specimens

The samples examined have the general formula $Al_{100}P_xV_y$-600 where $x, y = 0$, 5, 10, 20; and 600 corresponds to the final firing temperature (°C). The preparation procedure was as follows: known amounts of $Al(NO_3)_3 \cdot 9H_2O$ (Merck p.a.) and H_3PO_4 (Ferak p.a.) were dissolved in 250 ml of distilled water and V_2O_5, dissolved in 10 ml NH_4OH, was added. Then an ammonia solution (Ferak p.a.) was added gradually under stirring up to pH 9.5. The formed gel was dried at 110 °C for 24 h. Since previous thermogravimetric studies[23] had shown that such gels lose mass around 300–350 °C and stabilize their

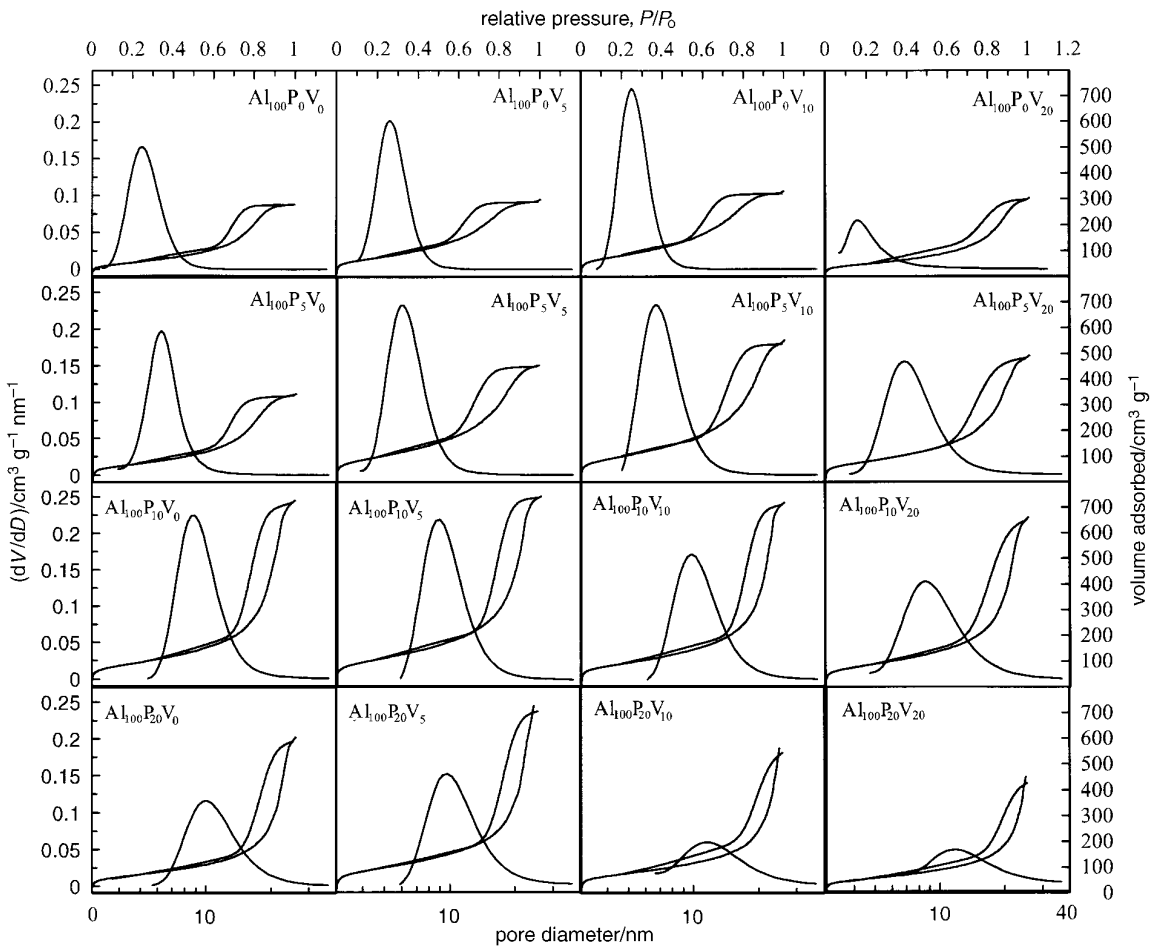

Fig. 2 Adsorption–desorption isotherms (N_2, 77 K) in Al—P—V—O mesoporous solids and the corresponding pore size distributions (BJH)

mass above this temperature, heating at this region was carried out very slowly in a tubular furnace under atmospheric conditions. The final firing temperature was set to 600 °C for a 6 h period.

The sixteen samples prepared and some of their properties are listed in Table 1.

XRD

The XRD patterns of the dried samples were recorded in a Siemens automatic diaffractometer and results are shown in Fig. 1.

Surface and porosity

The pore size distribution measurements were carried out using a Fisons Sorptomatic 1900 instrument. The characterization techniques included the determination of nitrogen adsorption–desorption isotherms from which the pore size distributions were also found (Fig. 2). The calculated surface areas and pore volumes are cited in Table 1 and shown in three-dimensional histograms in Fig. 3. In the same figure the separate as well as the cumulative action of P and V on the specific surface areas is shown.

SEM–EDX studies

The prepared samples were photographed to determine their morphology in a SEM system equipped with an EDX facility (JOEL 840-LINK AN IOS with a Be window). A selection of SEM photographs taken is shown in Fig. 4.

The samples were analysed for their surface composition by the EDX facility of the SEM system, each result being the average of ten measurements for each element Al, P, and V. The results are compared with the nominal composition of the samples in Fig. 5 as discussed in the next.

Discussion

The X-ray diffraction patterns shown in Fig. 1 indicate that the originator solid $Al_{100}P_0V_0$ exhibits the typical crystal structure of γ-Al_2O_3. Gradual incorporation of vanadium at 5 and 10%, results in a formation of less crystalline solids, while addition of 20% results in the reformation of the well crystallized original solid (γ-Al_2O_3) but additionally some extra very sharp peak due to V_2O_5 become apparent. Clearly vanadium oxide in excess of 10–15% cannot be incorporated into the structure of γ-Al_2O_3 and remains in a separate phase. This is clear also in the samples $Al_{100}P_5V_{20}$ and $Al_{100}P_{10}V_{20}$. Addition of phosphorus into the original solid $Al_{100}P_0V_0$ results in gradual formation of increased amounts of amorphous materials (see for example samples $Al_{100}P_5V_0$ and $Al_{100}P_{10}V_0$) while the addition of *ca.* 20% P (sample $Al_{100}P_{20}V_0$) results in the formation of a $AlPO_4$ crystal phase (broad peak at 2θ *ca.* 25°). Similar results were observed previously[21,22] indicating the ability of phosphorus to transform the crystalline γ-alumina into an amorphous solid, but with much higher surface area. The present results indicate that the action of vanadium is not so profound in terms of its ability to destroy the crystallites of γ-Al_2O_3, but acts more midly in this direction in synergy with phosphorus.

This synergistic action of P and V is more profound in terms of their influence on the BET surface area of the solids (Fig. 3). Clearly the addition of P at constant concentration of V, and/or the addition of V at constant concentration of P, increases the specific surface area considerably, the maximum

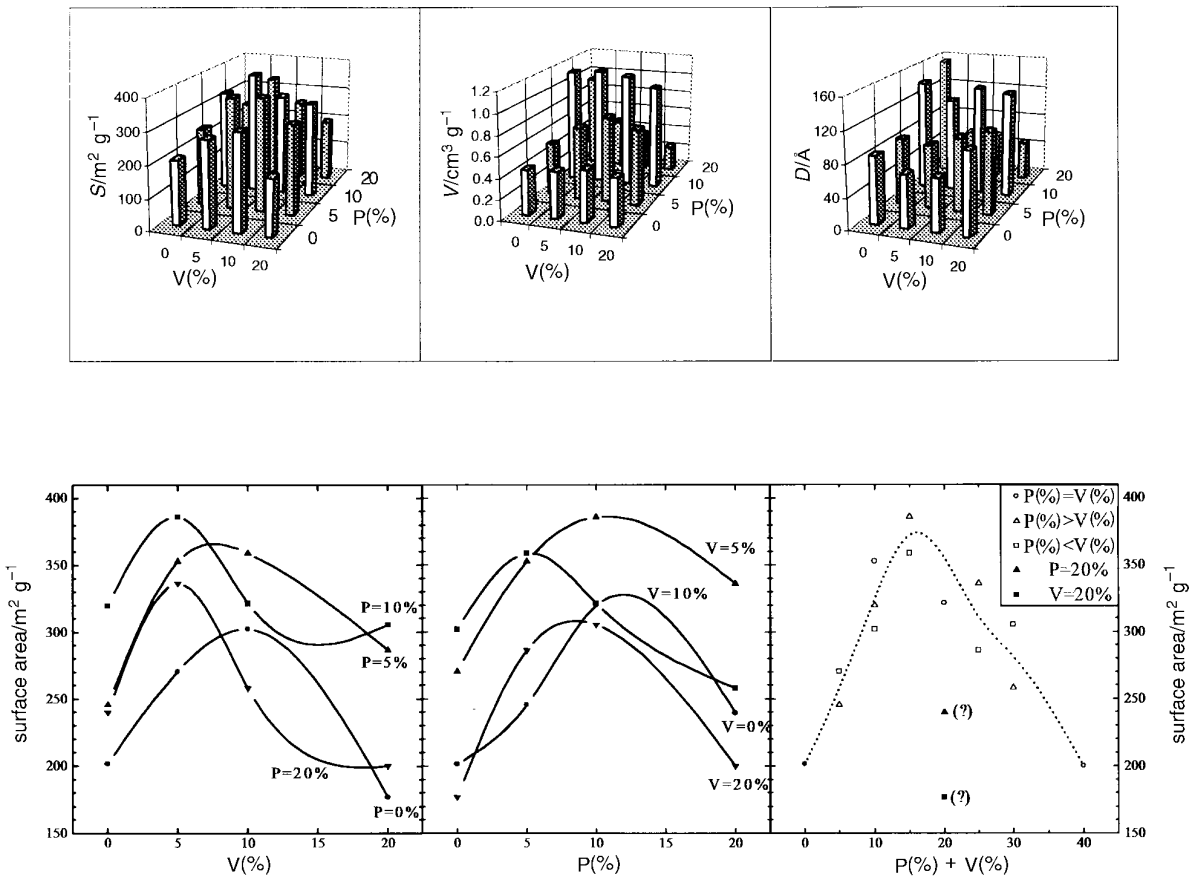

Fig. 3 Upper: variation of the specific surface areas, the pore volume and the mean pore diameter of Al—P—V—O solids as a function of their composition. Lower: influence of the separate and synergistic action of P and V on the surface area of the solids A—P—V—O.

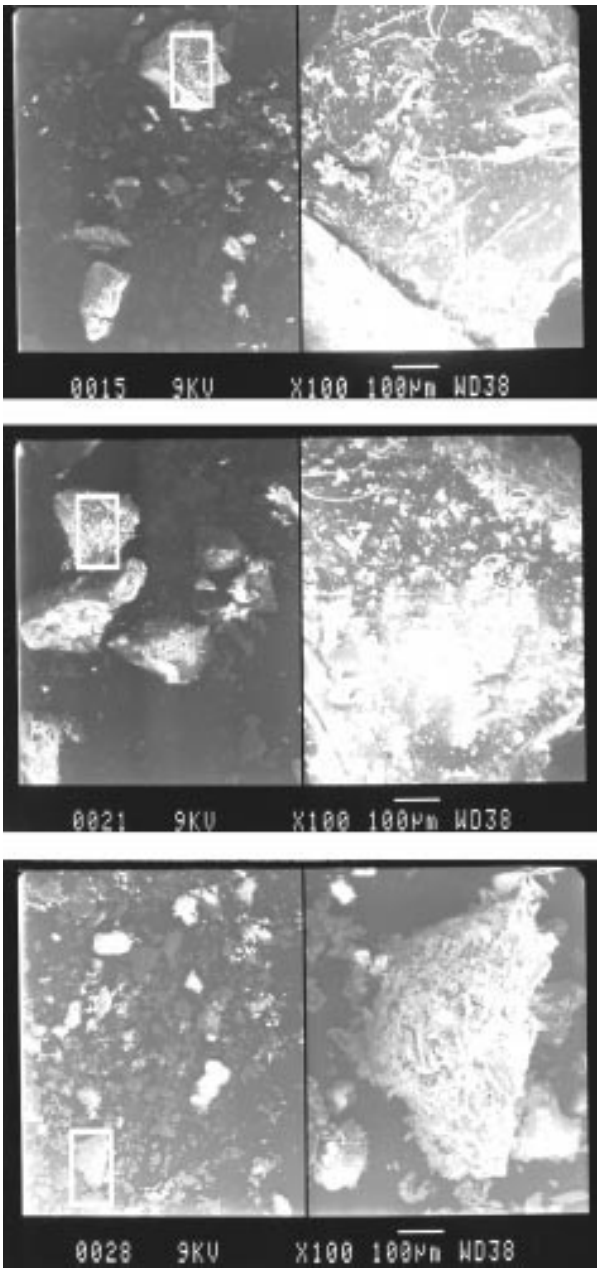

Fig. 4 Typical SEM photographs of Al—P—V—O solids

is achieved at 5–10% addition of each element. The synergistic action of the two elements is better seen in the lower right hand part of Fig. 3. Clearly the maximum effect is apparent at 15% cumulative addition of the two elements, while the influence of phosphorus is more significant than that of vanadium.

The adsorption–desorption loops of N_2 at 77 K and the calculated pore size distribution, shown in Fig. 2, indicate the dramatic influence caused by P and/or V on the porosity of the solids. The p.s.d.s shown in Fig. 2 have been approximated by a Gaussian and/or Lorentzian distribution as described in ref. 21 and 22. The corresponding results are given in Table 1 together with the FWHM of the distribution as well as the χ^2 criterion for the goodness of fit of the experimental p.s.d. with the x% Gaussian + (100-x)% Lorentzian approximation. The methodology applied was similar to that used in ref. 21 and 22. Briefly, a simulation computer program able to approximate different distributions by using the Gaussian or Lorentzian forms or chosen mixtures of both, was used. The goodness of fit was routinely tested *via* the objective function $\chi^2=\Sigma(\Delta y_i/\sigma_i)^2$ where Δy_i is the difference between the experimental and calculated data values of the ith point, and σ_i is the standard deviation. Optimisation in order to minimize χ^2 was performed by choosing, *via* trial and error methods in 5% steps, the optimum values of the Gaussian and Lorentzian contributions fitting the experimental points.

We observe (Fig. 2 and histogram in Fig. 3), that the maximum porosity is achieved at 10% addition of phosphorus, where pore volumes $>1\ cm^3\ g^{-1}$ are achieved. Addition of excess of P and/or V (>20%) decreases the porosity and drives the maximum of the p.s.d. at higher values. At the same time the p.s.d. becomes more spread. To quantify these results we have approximated the distribution by their Gauss and Lorentz components as shown in Fig. 6. It is clear that the addition of P, and to a less degree that of V, decreases the Gaussian component of the distribution and increases the Lorentzian component. At the same time the FWHM, a quantity reflecting the narrowness of distribution, changes in a controllable manner. The narrowest p.s.d. is achieved in the samples $Al_{100}P_0V_5$ and $Al_{100}P_0V_{10}$ where FWHM = 2.1 nm. The general picture emerging is that the distribution of the diameter of the pores can be manipulated in the mesoporous region between 5.0 and 13.0 nm by the controlled addition of P and/or V.

The crystal morphology of the solids, as seen by SEM magnification at 1–10 μm resolution (Fig. 4), shows interesting modification of the crystallites upon addition of P and/or V. Thus, crystallites of $Al_{100}P_{10}V_0$ (Fig. 4) possess an external surface which appears much more fragmented compared to the $Al_{100}P_0V_0$ sample (not shown) while sample $Al_{100}P_{20}V_0$ appears compact again. The same behaviour is seen for the addition of V; for the sample $Al_{100}P_0V_{10}$ the surface shows additional decorated patterns (Fig. 4) compared to $Al_{100}P_0V_0$, while sample $Al_{100}P_0V_{20}$ appears more compact. These results indicate the transformation of the original crystalline solid γ-Al_2O_3 to a more amorphous material possessing higher surface area upon addition of P and/or V. This phenomenon is accompanied, as expected, by the formation of a more disintegrated surface of the solid. A distinct appearance can be also seen in samples with high content of P and/or V (*e.g.* $Al_{100}P_{20}V_{20}$). The crystallites of those solids appear much more rugged and a kind of layered structure now seems to be more prominent. This result is not surprising given the well known layered structure of many phosphate and vanadate salts.

EDX surface analysis for Al, P and V is shown in Fig. 5. In this figure the ratios between experimental and theoretical content of the solids has been plotted *vs.* the nominal P and V content. The experimental values were those found by EDX while the theoretical are the ones calculated from the original synthesis. We observe that this ratio is around unity for Al, consistently above unity for P while for V the points are scattered, although the average values are also above unity. Those results indicate that phosphorus is accumulated on the surface of the solid by an amount as high as 30–40% as compared to an ideal uniform distribution at low addition of P and/or V but it lowered to 10–20% accumulation as the concentration of P and/or V is increased to 20%. Similar phenomena have been indirectly concluded in ref. 22 on the basis of ^{31}P MSD NMR observations but are clearly seen in the present work by the EDX analysis. The case of vanadium is not as clear as to the accumulation or depletion of this element on the surface. The points appeared scattered (right-hand site of Fig. 5) although the average value for each composition is above unity. This behaviour is most probably due to the non-homogeneous distribution of vanadium on the surface of the solids, which results in less precise and less consistent analytical identification of its composition.

Finally for Al, as expected, the experimental values match almost exactly the nominal composition. We note that an accumulation of P and/or V on the surface should result to

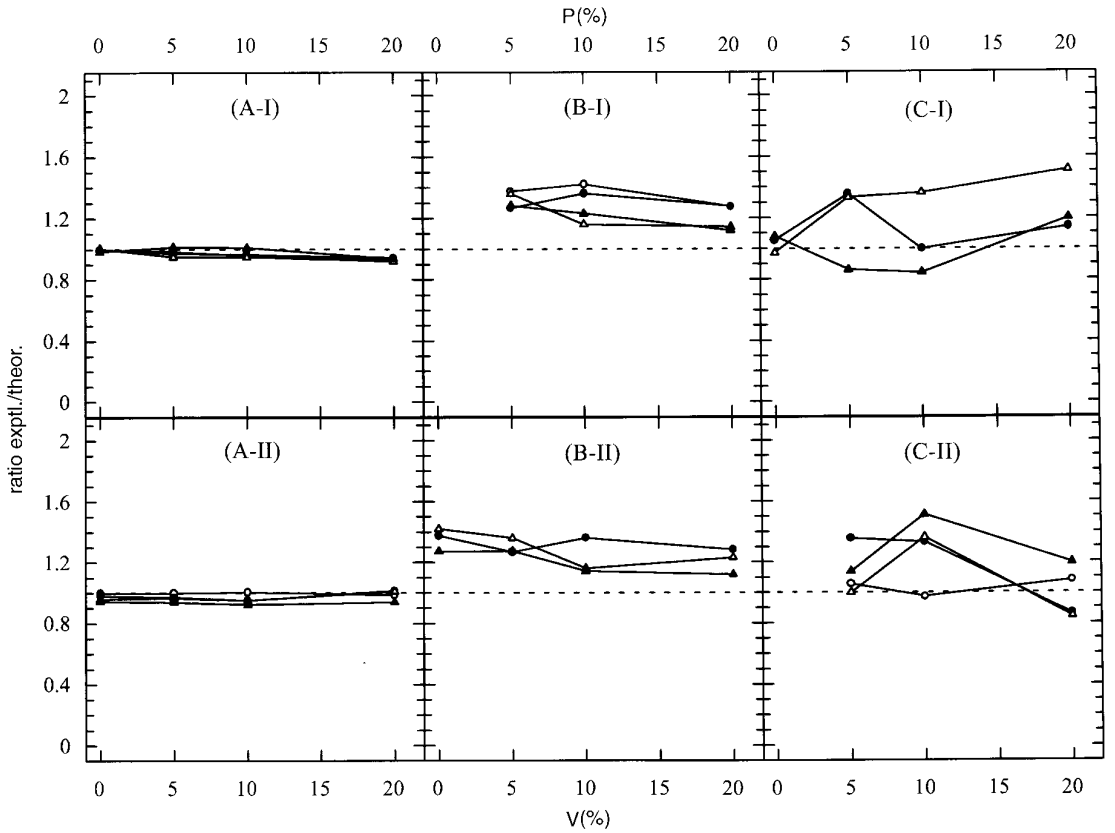

Fig. 5 Surface enrichment of Al—P—V—O solids for Al (A), P (B) and V (C) as a function of P (%) (I) or V (%) (II) content according to EDX analysis

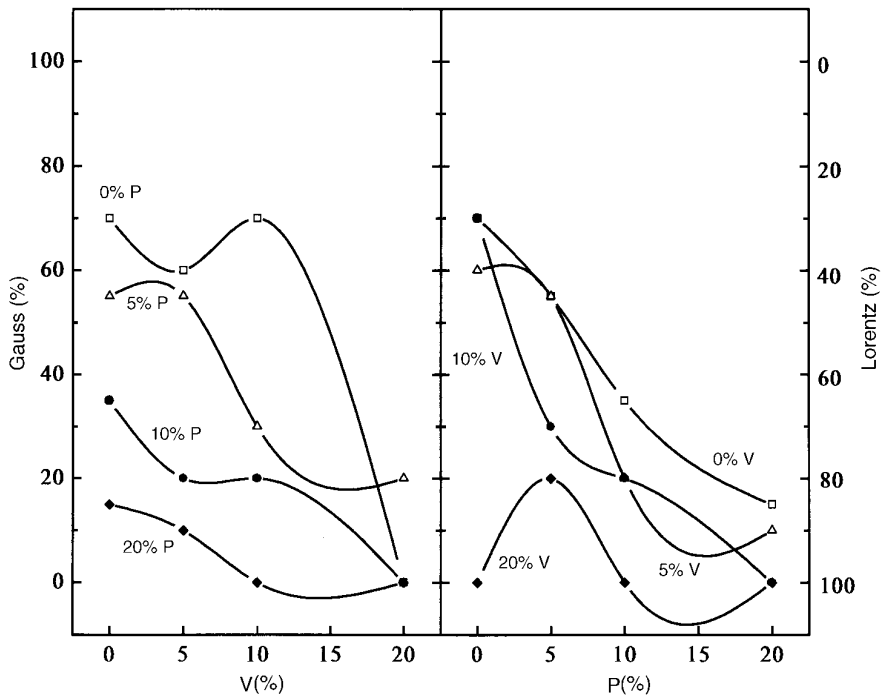

Fig. 6 Variation of the Gauss and Lorentz components of the p.s.d. shown in Fig. 2 as a function of P and V content

an equal depletion of Al in the bulk, however, since its concentration in the sample is much larger compared to the added elements, the resulting variation/depletion is much less noticeable. For example, for sample $Al_{100}P_{10}V_0$ an accumulation of P by 30% on the surface would result in a 'surface solid' of nominal composition $Al_{97}P_{13}V_0$ so the Al depletion would be only 3%.

In Fig. 6 the p.s.d. $dV/dD=f(D)$ depicted in Fig. 2 is approximated according to the % Gaussian and/or Lorentzian component of the distribution calculated similar to the method used

in ref. 21 and 22 as mentioned previously. In agreement with the data in ref. 21 and 22 for similar Al–P–O mesoporous solids, the addition of phosphorus decreases the % Gaussian component and increases the corresponding Lorentzian component (Fig. 6). This effect indicates that the formation of pores is become less random, around its most probable values, as %P increases. The same effect, but less regular, is observed upon addition of vanadium (Fig. 6). The reason might be again the rather uneven distribution of vanadium on the background of alumina as detected by EDX. This uneven distribution may originate from the possibility that the vanadium is not necessarily existing in a fixed oxidation state. Drying, may result in the formation of different concentrations across the surface and, as a result, in a differentiated influence on the formation of pores. Therefore the influence of adding vanadium to give a more Lorentzian distribution of pores is clear (Fig. 6) but less controlled, compared to phosphorus.

A depiction of the above description of alumina-aluminium phosphate (AAP) solids is given in Fig. 7. The introduction of 15–20% P to the original solid in the form of PO_4^{3-} groups results in solids with maximum ssa and porosity. The important point is that the P atoms are not evenly distributed but are accumulated on the surface as shown in Fig. 7(*)* (the surface is at the top of the picture). Further increased addition of P results in the formation of $AlPO_4$ [Fig. 7(*b*)]. It can be easily envisaged that in a 10×10 matrix of $Al_{80}P_{20}O_{100}$ groups similar to that shown in Fig. 7 and in which the P atoms are evenly distributed in two-dimensional space, that each P atom has no P atoms in the eight nearest-neighbour positions but it has four P atoms in the 18 next-to-the-nearest-neigbour available positions. However in the three-dimensional solid $Al_{80}P_{20}O_{100}$ each P atom should have three to four next-neighbour P atoms in the 24 available positions as can be easily verified. So the limit of maximum ssa and the porosity appears at the point where the phosphorus atoms start having three-ti-four next-neighbour atoms *i.e.* start coordinating to other P atoms. Alternatively, the limit of maximum ssa and porosity appears at *ca.* 17–18% substitution of Al by P which corresponds to one P atom in one of the corners of the octahedron surrounding each Al atom. This can be regarded as a percolation threshold where the formed chains Al—O—P—O—Al—O—P are practically infinite in length corresponding to the so-called percolation cluster [24] zigzagged all around the surface of each particle. The percolation threshold in a bcc lattice is 0.1803[24] in full agreement with the present observations.

In Fig. 7(*a*), which depicts the accumulation of phosphate on the surface of the solids (see Fig. 5), each P atom has at least one nearest-neighbour atom in two-dimensional space, while in three dimensions there should be eight to twelve next-neighbour P atoms of the 24 available positions, and therefore the $AlPO_4$ structure [Fig. 7(*b*)] starts to form in the outer shell of the solid particles. In other words, it seems that the gradual addition of P, results in the development of the $AlPO_4$ crystal phase from the outer towards the inner part of the Al_2O_3 particles which are eventually transformed to $AlPO_4$ [Fig. 7(*b*)].

The situation for vanadium is rather different and its distribution on the solid is not statistically even but rather islands of VO_x are formed and a few V atoms are incorporated into the Al_2O_3 structure, while the formation of $VOPO_4$ groups might also take place as shown by the synergistic action of V and P in increasing the ssa and porosity (see Fig. 3) of the AlPV solids.

Conclusion

This work has shown that addition of vanadium as well as mixtures of vanadium and phosphorus into alumina gels results, after drying, in the formation of mesoporous amorphous solids. Both elements contribute to an increase of surface area and porosity but the influence of P is more regular and predictable than that of vanadium. A synergistic effect is observed between the two elements in terms of surface area

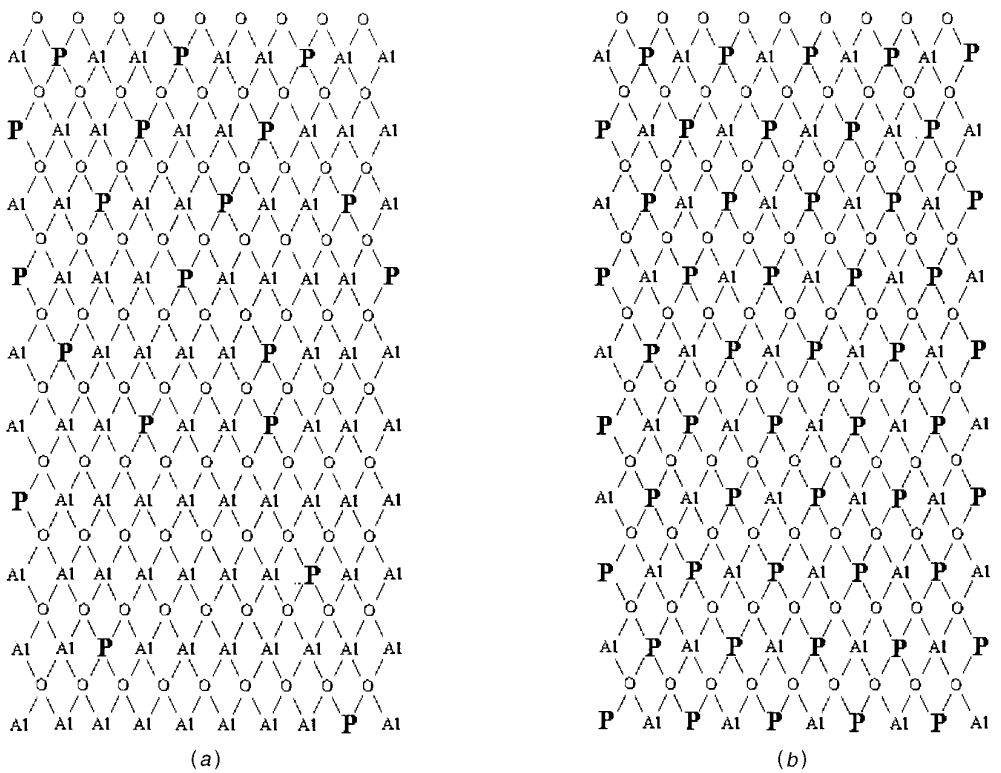

Fig. 7 Two-dimensional depiction of alumina–aluminum–phosphate (AAP) solids: (*a*) 10×10 matrix of $Al_{80}P_{20}O_{100}$ groups with accumulation of P atoms at the top; (*b*) 10×10 matrix of $Al_{50}P_{50}O_{100}$ groups ($AlPO_4$). For details see text.

and pore development which is maximised upon 15–20% addition of both. Phosphorus shows an homogeneous accumulation on the surface of the Al—P—V—O solids while vanadium shows a less regular distribution which might be due to variable oxidation state of vanadium, as in contrast to phosphorus, which may result in local variation of its surface concentration during drying and, as a result to less predictable surface effects.

We wish to thank Dr. E. Paulidou, SEM unit, University of Thessaloniki, for her help. Part of this work was supported from an HCM program of the EU, contact ERBCHQXCT 930272 and a TMR project, contact ERBFMRXCT 960084.

References

1 C. T. Kresge, M. E. Leonowicz, W. J. Roth, J. C. Vertulli and J. S. Beck, *Nature (London)*, 1992, **359**, 710.
2 J. S. Beck, J. C. Vartulli, W. J. Roth, M. E. Leonowicz, C. T. Kresge, K. D. Schmitt, C. T-W. Chu, D. H. Olson, E. W. Sleppard, S. B. McCullen, J. B. Higging and J. L. Schlenkev, *J. Am. Chem. Soc*., 1992, **114**, 10834.
3 C. M. Lambert and C. G. Granqvist in *Large-Area Chromogenics: Materials and Devices for Transittance Control*, ed. C. M. Lambert and C. G. Granqvist, 2–19 SPIE Optical Engineering, Washington DC, 1990.
4 W. C. Danternsont-Smith, *Displays*, 1982, **3**, 3.
5 J. Haggin, *Chem. Eng*., 1990.
6 R. F. Parton, J. M. Jacobs, H. van Ooteghens and P. A. Jacobs, in *Zeolites as Catalysts, Sorbents and Detergent Builders*, ed. H. G. Karge and J. Weitkamp, Elsevier, Amsterdam, 1989, pp. 211–212.
7 D. M. Antonelli and J. Ying, *Angew. Chem., Int. Ed. Engl*., 1996, **35**, 426.
8 D. Walsh and S. Mann, *Nature (London)*, 1995, **377**, 320
9 S. Oliver, A. Kupperman, N. Coombs, A. Lough and G. Ozin, *Nature (London)*, 1995, **378**, 47.
10 M. J. Hudson and J. A. Knowles, *J. Chem. Soc., Chem. Commun*., 1995, 2083.
11 M. J. Hudson and J. A. Knowles, *J. Mater. Chem*., 1996, **6**, 89.
12 U. Ciesla, S. Schacht, G. D. Stucky, K. K. Unger and F. Schuth, *Angew. Chem., Int. Ed. Engl*., 1996, **35**, 542.
13 P. T. Tanev, M. Chibwe and T. J. Pinnavaia, *Nature (London)*, 1994, **386**, 321.
14 D. M. Antonelli and J. M. Ying, *Angew. Chem., Int. Ed. Engl*., 1995, **34**, 2014.
15 P. Behrens, *Angew. Chem., Int. Ed. Engl*., 1996, **35**, 515.
16 P. Behrens and G. D. Stucky, *Angew. Chem., Int. Ed. Engl*., 1993, **32**, 696.
17 Q. Huo, D. I. Margolese, U. Ciesla, P. Feng, T. Gier, P. Sieger, R. Leon, P. M. Petroff, F. Schuth and G. D. Stucky, *Nature (London)*, 1994, **363**, 317.
18 P. Tanev and T. J. Pinnavaia, *Science*, 1995, **267**, 865.
19 A. Monnier, F. Schuth, Q. Huo, D. Kumar, D. Margolese, R. S. Maxwell, G. D. Stucky, M. Krishnamutry, P. Petroff, A. Fironzi, M. Janicke and B. F. Chmelka, *Science*, 1993, **261**, 1299.
20 *Multifunctional Mesoporous Materials*, ed. M. J. Hudson and C. A. C. Sequeira, NATO ASI vol.400, Kluwer, Dortrecht, 1993
21 D. E. Petrakis, M. J. Hudson, A. T. Sdoukos, P. J. Pomonis and T. V. Bakas, *Colloids Surf. A: Phys. Eng. Aspects*, 1994, **90**, 191.
22 D. E. Petrakis, M. J. Hudson. P. J. Pomonis, A. T. Sdoukos and T. V. Bakas, *J. Mater. Chem*., 1995, **5**, 1975.
23 K. M. Kolonia, D. E. Petrakis, T. C. Vaimakis, E. D. Economou and P. J. Pomonis, *Thermochim. Acta*, 1997, **3224**, 1.
24 D. Stanffer and A. Aharony, *Introduction to Percolation Theory*, Taylor and Francis, London, 2nd edn., 1994.

Paper 7/014339*B*; *Received* 28*th February*, 1997